JOURNAL OF AIRCRAFT
Vol. 46, No. 6, November–December 2009

Predicting Wall Pressure Fluctuation over a Backward-Facing Step Using Detached Eddy Simulation

Jean-François Dietiker*
West Virginia University Research Corporation, Morgantown, West Virginia 26506-6216
and
Klaus A. Hoffmann†
Wichita State University, Wichita Kansas 67260-0044

DOI: 10.2514/1.43912

Numerical simulations of a turbulent flow over a backward-facing step are performed. The governing equations are solved by the finite volume code Cobalt. Unsteady three-dimensional detached eddy simulations are carried out with Menter's shear stress transport turbulence model acting as a subgrid-scale model. Mean flow quantities such as pressure, velocity, and skin-friction coefficients are accurately predicted. Velocity and pressure fluctuations are resolved by the three-dimensional computations. The dominant frequency is in good agreement with existing experimental data, and power spectral analysis of wall pressure fluctuation is consistent with empirical relations found in the literature for several operating conditions.

Introduction

WALL pressure fluctuations beneath a turbulent boundary layer are associated with noise generation and can lead to structural vibrations. It is desirable to understand the nature of pressure fluctuations to limit their impact in several engineering applications such as commercial airplanes and turbines. Turbulent-boundary-layer measurement has been the subject of numerous investigations, and precious information can be obtained from experiments [1–7], which can be used to validate available semi-empirical models.

With the advent of computational fluid dynamics, numerical tools have been developed to study and understand a wide range of turbulent flowfields. There are mainly three approaches for the computation of turbulent flows. The direct numerical simulation approach is an exact method, in the sense that the original governing equations are solved without any modifications or filtering process. The second approach for turbulent flow computation is large eddy simulation (LES) [8]. Large scales are numerically computed, whereas small scales are modeled by simple eddy viscosity models, known as subgrid-scale models (SGS). Algebraic models are sufficient, because the imperfections of these simple models should not greatly affect the solution. The two methods described above are very costly in terms of computational time and storage requirement. A more affordable method consists of averaging the Navier–Stokes equations in time, resulting in the Reynolds-averaged Navier–Stokes (RANS) equations. A turbulence model is required to close the system. Several different turbulence models exist, ranging from simple algebraic models to more sophisticated multi-equation models [9–13]. A hybrid method has been recently developed to take advantage of existing techniques. Detached eddy simulation (DES) combines the RANS approach in regions of thin boundary layer where no separation occurs, because this does not constitute a real challenge for RANS and switches to LES in the region of massive separation [14]. This method allows a reduction of the prohibitive cost of the LES method, and the solution of a turbulent flowfield can therefore be obtained within a reasonable computational time.

Recently, direct numerical simulations of turbulent boundary layers have been performed, which provide insightful information such as turbulence statistics and frequency spectra [15]. Good agreement was found with the experimental work of Webster et al. [16]. Hu et al. [17] performed direct numerical simulation of turbulent-plane Poiseuille and Couette flows and studied fluctuating wall pressure and shear stresses. Good agreement with existing data was found.

However, direct numerical simulation requires extensive computational resources that are beyond the reach of industrial applications at the present time. The potential use of more economical approaches such as LES and DES for aeroacoustic predictions is discussed in [18]. Although they recommended LES-types methods over RANS methods, DES can provide useful results for three-dimensional flows in industrial applications. Ciardi and Dawes [19] studied four subgrid-scale models and different approaches to blend LES and RANS to perform broadband noise analysis in turbomachinery. Lee et al. [20] predicted wall pressure fluctuations using Reynolds-averaged Navier–Stokes equations along with an isotropic model. The prediction of the surface pressure spectrum was obtained by solving a Poisson equation for the fluctuating pressure in a turbulent boundary layer. Good results were obtained for a zero-pressure-gradient flow.

Pressure fluctuations beneath surfaces of discontinuities such as cavities or forward and backward steps have been the subject of many investigations [21–24]. They are typically associated with regions of separated flow. Flows over small steps are of interest in the aerospace community because they are sources of aerodynamic noise that propagates to the aircraft interior and can lead to structural vibration. The need to develop numerical tools to predict pressure fluctuations is therefore essential before noise-reduction techniques can be implemented. The objective of the current study is to numerically solve the flow over a backward-facing step using unsteady three-dimensional detached eddy simulation. Numerical results are compared to existing experimental results.

Governing Equations

The governing equations are the unsteady compressible Navier–Stokes equations, composed of the conservations of mass, momentum, and energy.

Continuity equation:

$$\frac{\partial \rho}{\partial t} + \nabla \cdot (\rho \mathbf{U}) = 0 \tag{1}$$

Received 18 February 2009; revision received 24 August 2009; accepted for publication 31 August 2009.

*Senior Research Engineer, 886 Chestnut Ridge Road, P.O. Box 6216; jeff.dietiker@mail.wvu.edu.

†Marvin J. Gordon Distinguished Professor Department of Aerospace Engineering, 1845 Fairmount; Klaus.hoffmann@wichita.edu.

Momentum equation:

$$\frac{\partial(\rho \mathbf{U})}{\partial t} + \nabla \cdot [\rho \mathbf{U} \otimes \mathbf{U} + p\bar{\bar{\mathbf{I}}}] = \nabla \cdot \bar{\bar{\tau}} \tag{2}$$

Energy equation:

$$\frac{\partial}{\partial t}(\rho e_t) + \nabla \cdot [(\rho e_t + p)\mathbf{U}] = \nabla \cdot (\mathbf{U} \cdot \bar{\bar{\tau}}) - \nabla \cdot \mathbf{Q} \tag{3}$$

Cobalt is the computational fluid dynamics code used to solve Eqs. (1–3). Cobalt is an unstructured finite volume commercial code using a cell-centered formulation. This compressible flow solver has been validated on several problems by Strang et al. [25] and Forsythe et al. [26]. Cobalt provides both RANS and DES approaches for turbulence modeling. The Spalart–Allmaras and Menter shear stress transport (SST) models are available and act as SGS models for DES. Details about the Cobalt algorithm may be found in [27,28]. Cobalt does not use a preconditioner for incompressible flow regimes. However, low Mach number flows have been accurately predicted, and the absence of a preconditioner did not adversely affect the solution [29].

The original DES concept was proposed in 1997 by Spalart et al. [30]. This technique blends LES and RANS formulation. It uses a single turbulence model, which functions as a subgrid-scale model in regions where the grid density is sufficiently fine for LES and functions as a RANS model in regions where it is not [31]. Originally, DES was based on the Spalart–Allmaras one-equation turbulence model [11]. In the LES region, the larger-scale eddies are resolved directly, and the smaller eddies are represented by the SGS model.

Traditional LES wall models may have difficulties to accurately resolve separated flows, and grid refinement could demand excessive computing power. Since RANS models are known to be cost-effective and have been fairly well developed to provide accurate boundary-layer calculations, they are used as a wall model in the near-wall region. On the other hand, in regions of highly separated flows, RANS models perform poorly, and LES is an attractive option to resolve large eddies. DES does not have an explicit filter operator similar to LES. The switching between RANS and LES depends on the grid spacing and can be controlled during the preprocessing stage. In the current investigation, detached eddy simulation is performed using Menter's SST two-equation turbulence model [13].

Menter's SST two-equation turbulence model is a combination of the k-ε and the k-ω turbulence models, and it uses the best features of both models. The model switches to the k-ω model in the inner region of the boundary layer and switches to the k-ε model in the outer region of the boundary layer. Therefore, the model will be well-behaved in the near-wall region and will stay insensitive to freestream conditions in the outer region of the boundary layer. The combined model is written such that both models are blended together through a switching function. The switching function F_1 is designed such that $F_1 = 1$ in the near-wall region to activate the k-ω model and $F_1 = 0$ at the boundary-layer edge to activate the k-ε model and ensure the freestream independence of the model. Menter's SST model is based on the assumption of the Johnson–King model, where the turbulent shear stress is proportional to the turbulent kinetic energy in the log and wake regions of the turbulent boundary layer. The eddy viscosity is limited by the turbulent kinetic energy to ensure the proportionality condition.

Results

The experimental results of Driver et al. [32,33] will be used to assess the accuracy of the computational results. Figure 1 illustrates the schematic of the flow over a backstep. The step height is $H = 1.27$ cm. The freestream Mach number is $M_\infty = 0.128$, and the incoming boundary-layer thickness is $\delta = 1.9$ cm. The Reynolds number, based on the step height and freestream velocity, is $Re_H = 37,000$. As the air flows over the backstep, a shear layer develops, the flow detaches, and a recirculation region is formed. The size of the recirculation region and reattachment point are time-dependent. A small corner eddy exists between the step and the main

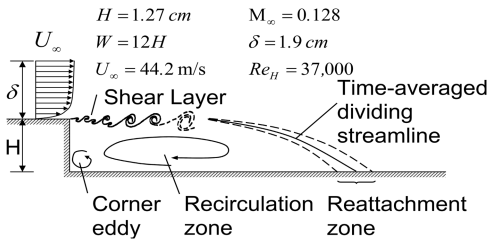

Fig. 1 Schematic of the backstep flow.

recirculation zone. In the experiment of Driver et al., the width of the step is equal to 12 step heights, and the upper wall of the wind tunnel is located nine step heights away from the lower wall. Available experimental data consist of mean velocity profiles, turbulent kinetic energy profiles, mean wall pressure, and skin-friction coefficients. Uncertainties on measurements are 4% on velocity, 15% on turbulent kinetic energy, ± 0.009 on pressure coefficient, and 8% on skin-friction coefficient (15% in the separated region).

Unsteady three-dimensional computations are carried out using detached eddy simulation along with Menter's SST turbulence model, acting as a subgrid-scale model. Results obtained with a two-dimensional Reynolds-averaged turbulence model did not provide any pressure fluctuation due to the inherent time-averaging formulation. Therefore, only three-dimensional DES results are presented. The grid system is illustrated in Fig. 2. The domain extends four step heights upstream of the step. Incoming velocity profile and turbulent kinetic energy profiles are prescribed at the inlet and match the experimental data of Driver et al. [32,33]. The upper wall is located nine step heights from the lower wall. The channel outlet is located 50 step heights downstream of the step. The domain extends 12 step heights in the spanwise direction. Heavy clustering is implemented near the lower and upper walls to capture the boundary layer and near the step to capture the recirculation region and reattachment zone. The clustering has been adjusted such that the first value of y^+ away from the wall is less than one along the lower and upper walls. Three structured grid systems have been investigated: coarse (238,000 cells), medium (767,000 cells), and fine (1.9 million cells). Results obtained with the medium and fine grids were practically identical. Time averages were calculated after the flow had time to sweep the computational domain twice. Time statistics were taken for a total duration of 1 s. All computations were performed on one of the clusters available at Wichita State University's High Performance Computing Center. A typical run took two to three days to complete, using 16 processors. Although no direct comparisons with LES results were performed due to the nonavailability of an LES code, typical DES results can be obtained 10 to 12 times faster than LES results [34].

Figure 3 shows averaged streamline pattern near the backstep along the center plane. The background is colored by the x-velocity component. The corner eddy and main recirculation regions are clearly identifiable. The location of the reattachment is well predicted by the computation. The reattachment length is $x/H = 6.0$, which

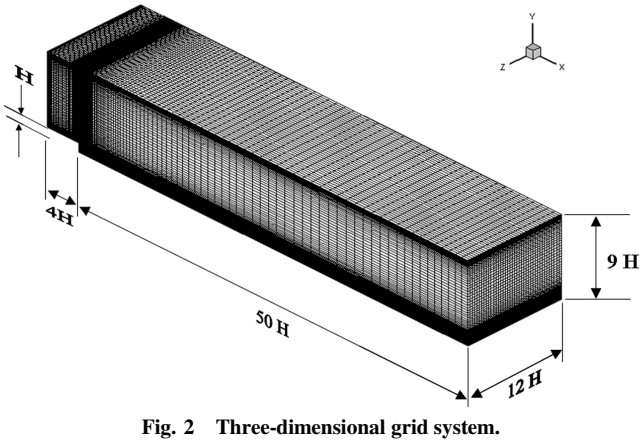

Fig. 2 Three-dimensional grid system.

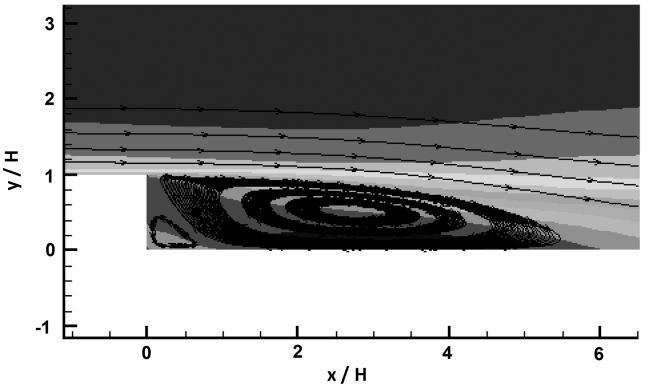

Fig. 3 Streamline pattern downstream of the corner along the center plane.

compares well with the measurements ($x/H = 6.2$ by oil-flow laser interferometer and $x/H = 6.05$ by thermal tuft).

Distributions of wall static pressure coefficients are presented in Fig. 4 along the lower wall (step sidewall) and upper wall (opposite side). Good agreement is found between the current computation and the experimental results. The influence of the step is evident by comparing the pressure distributions along the lower and upper walls. The pressure gradient is larger on the step sidewall and is the largest near the reattachment point.

Figure 5 shows the step-side skin-friction coefficients. Excellent agreement is obtained with the experimental data. The size of the recirculation region is well predicted, and the small corner eddy is confined within less than one step height form the corner.

Figure 6 illustrates mean velocity profiles in the separation and reattachment regions. Good agreement is obtained with the experiments. The velocity gradient is approximately constant across the shear layer. The velocity distribution is particularly well predicted inside the recirculation region. Results obtained with the fine grid are also included to show the effect of grid refinement. Results are shown to be practically grid-insensitive.

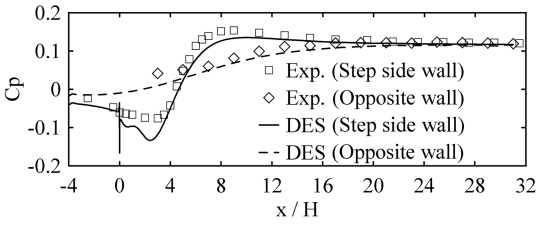

Fig. 4 Wall pressure coefficients.

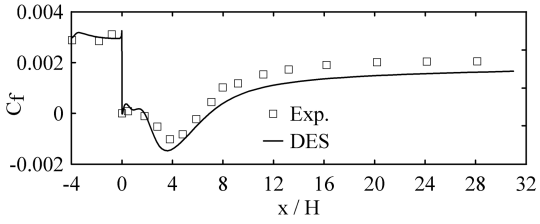

Fig. 5 Skin-friction coefficients (step sidewall).

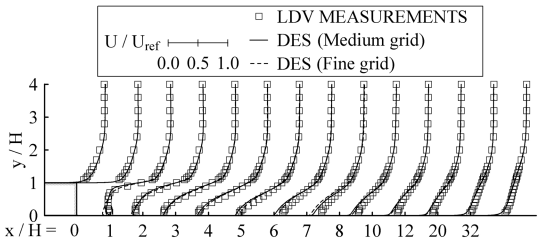

Fig. 6 Velocity profiles along the center plane (LDV denotes laser Doppler velocimetry).

The modeled turbulent kinetic energy profiles are shown in Fig. 7. The modeled turbulent kinetic energy is one of the working variables associated with the k-ε and the k-ω turbulence models. It is computed by solving an additional transport equation based on time-averaged quantities. The numerical results are in fairly good agreement with the measured values. A sudden increase in turbulent kinetic energy is observed in the shear layer, just downstream of the step, followed by a moderate increase over the next five step heights. The computation tends to underestimate the maximum values of the turbulent kinetic energy within the recirculation region. Further downstream, the level of kinetic energy decreases as the flow reattaches. Discrepancies between the computed and measured values are also diminishing far away from the step.

The resolved turbulent kinetic energy, which is explicitly computed from the unsteadiness of the flowfield, is presented in Fig. 8. The ability to accurately capture velocity fluctuations is crucial to predict pressure fluctuations. Turbulence models used in RANS methods are not able to explicitly capture velocity fluctuations. The advantage of the detached eddy simulation is the possibility to resolve those velocity fluctuations. Good accuracy is obtained up to three step heights away from the step. Further downstream, the turbulent kinetic energy underpredicts the experimental values but is more accurate than the modeled turbulent kinetic energy. This is encouraging and suggests that DES may provide adequate information related to pressure fluctuation prediction.

Although this type of flow is classified as a two-dimensional flow, when averaged in time, instantaneous three-dimensionality of the flowfield can be identified in Fig. 9. Figure 9a shows an isodensity surface and the shape of the shear layer and Fig. 9b shows an instantaneous view of the recirculation region.

Figure 10 shows the time history of the surface pressure at $x/H = 5.5$. Large pressure fluctuations are observed. The energy spectrum of the surface pressure is shown in Fig. 11. Most of the energy resides at the nondimensional frequency $n = fL/U_{\text{ref}} = 0.582$, which compares well with the experimental value of $n = 0.6$. Time history of the streamwise velocity component at $x/H = 6$ and $y/H = 1$ is depicted in Fig. 12. Results are comparable to the experimental data, although the maximum nondimensional velocity is underpredicted (0.75 in the current computations versus 0.9 in the experiments). The energy spectrum of the streamwise velocity component is shown in Fig. 13. The dominant nondimensional frequency of $n = 0.59$ compares well with the experiment ($n = 0.6$).

Figure 14 shows wall pressure fluctuations along the lower wall. A rapid increase is observed downstream of the step. The maximum is

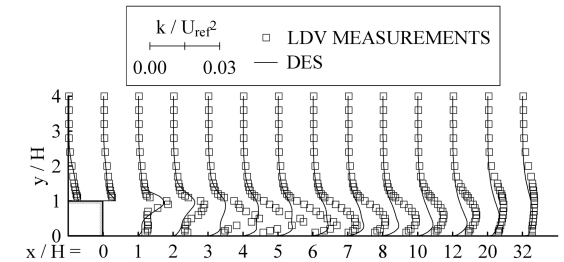

Fig. 7 Modeled turbulent kinetic energy along the center plane.

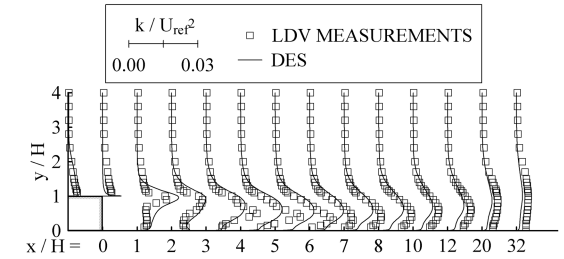

Fig. 8 Resolved turbulent kinetic energy along the center plane.

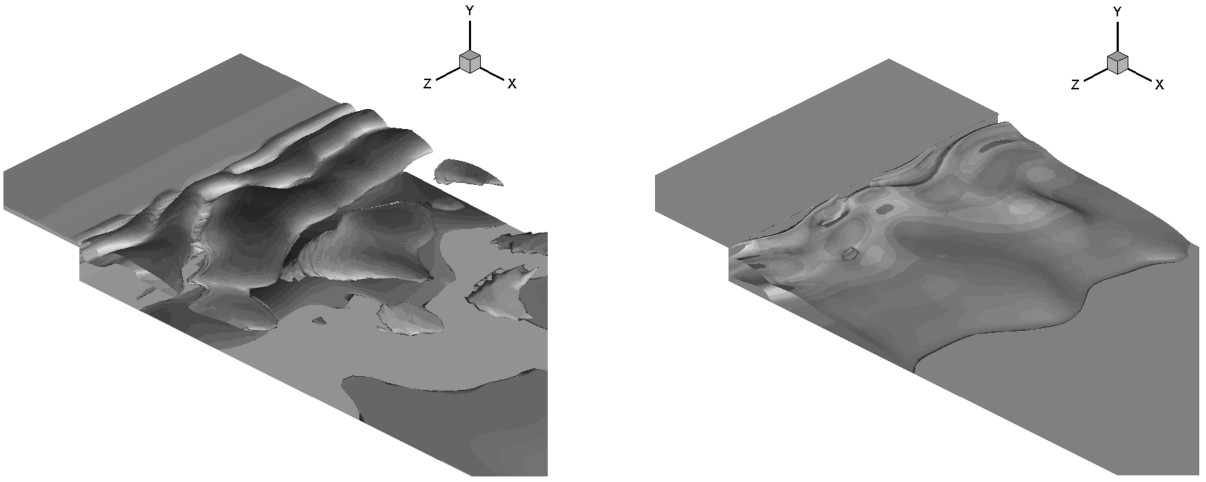

a) Iso-density surface b) Recirculation region

Fig. 9 Instantaneous view of the flow structure.

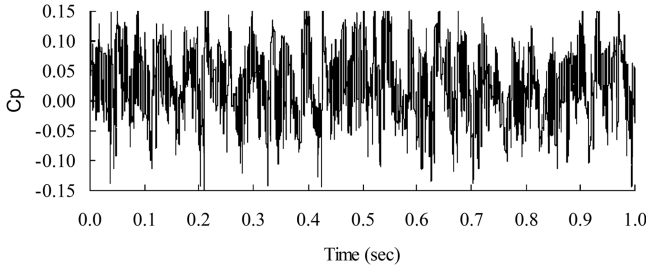

Fig. 10 Time history of surface pressure.

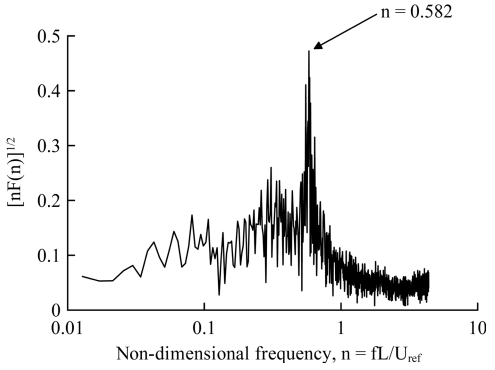

Fig. 11 Pressure frequency spectrum.

reached at about five step heights away from the corner and is followed by a rapid decrease until $x/H = 12$. Further downstream, a steady decrease in pressure fluctuation is observed. The location of the maximum is consistent with values found in the literature [23].

Next, it is attempted to correlate the current results with the empirical relations proposed by Efimtsov et al. [23]. Based on a series of experiments conducted for flows over backward-facing steps of different heights under several flow conditions, Efimtsov et al. generalized the experimental results and proposed a pressure fluctuation spectrum in the following form:

$$\phi(x,\omega) = \frac{q^2 H}{U} F_m \psi(M) e^{-|x-x_m|/L} + \phi_{\mathrm{BL}}(\omega) \tag{4}$$

$$F_m = \frac{F_{m0}}{[(Sh/Sh_1)^{2n_1} + (Sh/Sh_2)^{2n_2}]^{1/2}} \tag{5}$$

Details about the formulation can be found in [23]. The typical spectrum is composed of two characteristic regions: 1) an energy-carrying region where the power spectral density reduces moderately as the frequency (or Strouhal number) increases and 2) a high-frequency region where the pressure fluctuations decrease rapidly with an increase in frequency. The proposed empirical relation contains the correction term $\psi(M)$ to include the effect of the Mach

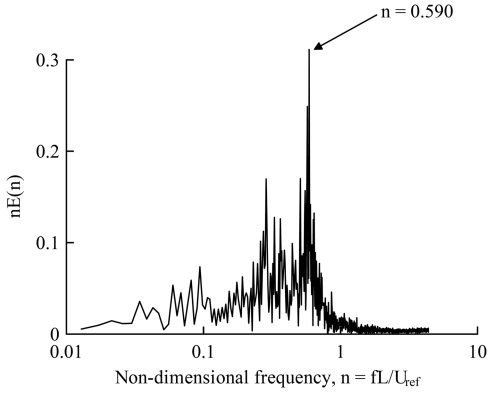

Fig. 13 Velocity frequency spectrum.

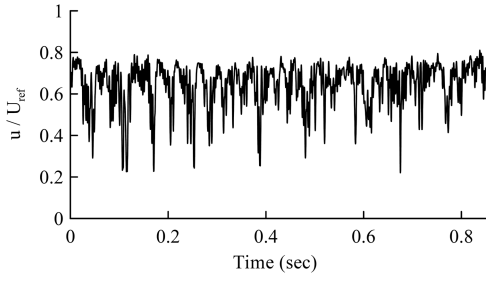

Fig. 12 Time history of velocity.

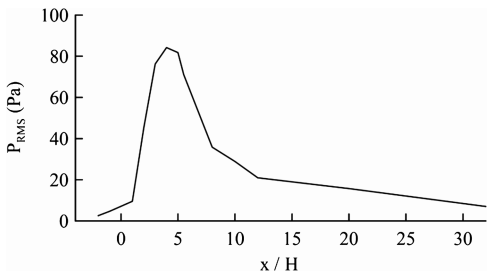

Fig. 14 Surface pressure fluctuations.

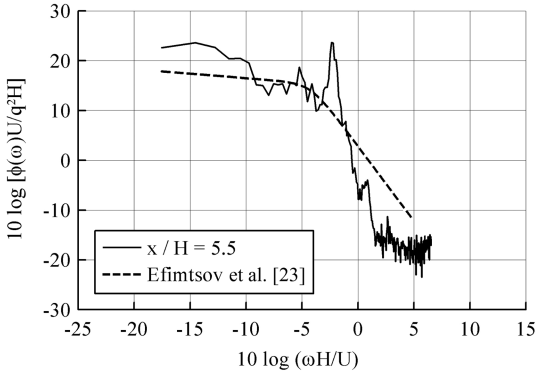

Fig. 15 Power spectral density (Efimtsov et al. [23]).

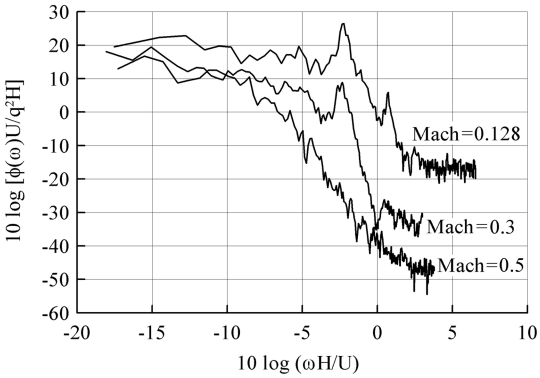

Fig. 16 Effect of Mach number on the power spectral density.

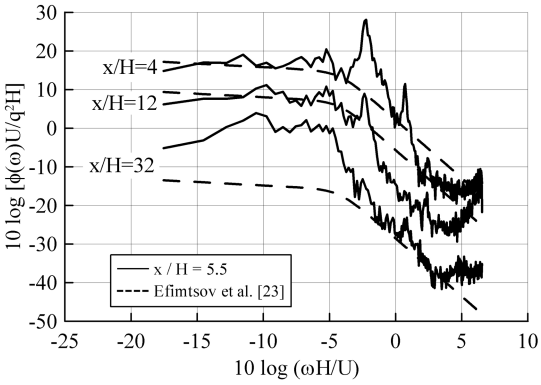

Fig. 17 Effect of position on the power spectral density (Efimtsov et al. [23]).

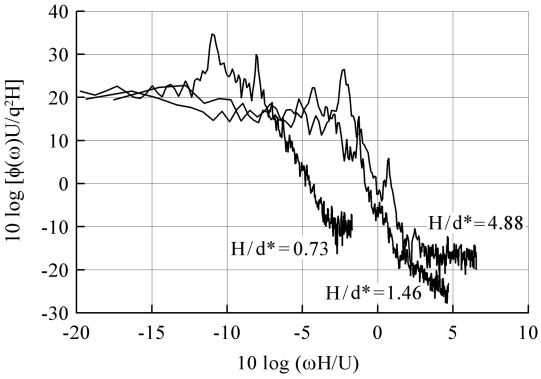

Fig. 18 Effect of step height on the power spectral density.

number and an exponential term to damp out the pressure fluctuations away from its maximum location. The term $\phi_{BL}(\omega)$ represents the spectral density of wall fluctuations of a turbulent boundary layer on a smooth surface with no pressure gradient. The function F_m allows a smooth transition between the two asymptotic lines. Figure 15 shows the power spectral density at $x/H = 5.5$. The general trend of the Efimtsov et al. [23] empirical relation is observed. The effect of the Mach number on the power spectral density is illustrated in Fig. 16. As the Mach number increases from 0.128 to 0.5, the spectrum is shifted toward lower frequencies. These results differ from the Efimtsov et al. relation, which predict a Mach-number-insensitive spectrum for Mach numbers lower than 0.8. Next, the effect of position on the power spectral density is investigated (Fig. 17). The general trend is consistent with the empirical relations, as the spectral densities decrease substantially away from the location of maximum pressure fluctuations. Finally, the influence of the step height is illustrated in Fig. 18. As the step height increases, the region of sharp decrease is shifted toward larger frequencies.

Conclusions

Unsteady three-dimensional detached eddy simulations have been performed to solve the flow over a backward-facing step using the finite volume flow solver Cobalt. Menter's shear stress transport turbulence model was used to close the system of equations. The computations were able to accurately predict mean pressure, velocity, skin-friction coefficient, and reattachment length. Menter's SST turbulence model was able to provide fairly accurate modeled turbulent kinetic energy. Resolved eddies were captured by the detached eddy simulation and provided information about velocity and wall pressure fluctuations. The frequency content matched the experimental results, and power spectral density analysis compared well with existing empirical relations for similar configurations.

Acknowledgments

The authors wish to thank the efforts of Judith Gallman and Mark Moeller of Spirit AeroSystems during the research program. All computations were performed at the High Performance Computing Center (HiPeCC) at Wichita State University.

References

[1] Sherman, C. H., Ko, S. H., and Buehler, B. G., "Measurement of the Turbulent Boundary Layer Wave-Vector Spectrum," *Journal of the Acoustical Society of America*, Vol. 88, No. 1, July 1990, pp. 386–390. doi:10.1121/1.400347

[2] Abraham, B. M., and Keith, W. L., "Direct Measurements of Turbulent Boundary Layer Wall Pressure Wavenumber-Frequency Spectra," *Journal of Fluids Engineering*, Vol. 120, March 1998, pp. 29–39. doi:10.1115/1.2819657

[3] Kim, J., "On the Structure of Pressure Fluctuations in Simulated Turbulent Channel Flow," *Journal of Fluid Mechanics*, Vol. 205, 1989, pp. 421–451. doi:10.1017/S0022112089002090

[4] Manoha, E., "The Wavenumber-Frequency Spectrum of the Wall Pressure Fluctuations Beneath a Turbulent Boundary Layer," AIAA Paper 96-1758, May 1996.

[5] Howe, M. S., "On the Structure of the Turbulent Boundary-Layer Wall Pressure Spectrum in the Vicinity of the Acoustic Wavenumber," *Proceedings of the Royal Society of London, Series A: Mathematical and Physical Sciences*, Vol. 412, No. 1843, 1987, pp. 389–401. doi:10.1098/rspa.1987.0093

[6] Arguillat, B., Ricot, D., Robert, G., and Bailly, C., "Measurements of the Wavenumber-Frequency Spectrum of Wall Pressure Fluctuations Under Turbulent Flows," AIAA Paper 2005-2855, May 2005.

[7] Leclercq, D. J. J., and Bohineust, X., "Investigation and Modelling of the Wall Pressure Field Beneath a Turbulent Boundary Layer at Low and Medium Frequencies," *Journal of Sound and Vibration*, Vol. 257, No. 3, 2002, pp. 477–501. doi:10.1006/jsvi.2002.5049

[8] Lesieur, M., and Comte, P., "Large Eddy Simulations of Compressible Turbulent Flows," Turbulence in Compressible Flows, AGARD Rept. 819, Neuilly-sur-Seine, France, 1997.

[9] Hoffmann, K. A., and Chiang, S. T., *Computational Fluid Dynamics*,

3rd ed., Vol. 2, Engineering Education Systems, Wichita, KS, 1998.
[10] Baldwin, B. S., and Lomax, H., "Thin Layer Approximation and Algebraic Model for Separated Turbulent Flows," AIAA Paper 78-257, Jan. 1978.
[11] Spalart, P. R., and Allmaras, S. R., "A One-Equation Turbulence Model for Aerodynamic Flows," AIAA Paper 92-0439, Jan. 1992.
[12] Jones, W. P., and Launder, B. E., "The Calculation of Low-Reynolds-Number Phenomena with a Two-Equation Model of Turbulence," *International Journal of Heat and Mass Transfer*, Vol. 16, No. 6, 1973, pp. 1119–1130. doi:10.1016/0017-9310(73)90125-7
[13] Menter, F. R., "Two-Equation Eddy-Viscosity Turbulence Models for Engineering Applications," *AIAA Journal*, Vol. 32, No. 8, 1994, pp. 1598–1605. doi:10.2514/3.12149
[14] Spalart, P. R., "Strategies for Turbulence Modeling and Simulations," *Engineering Turbulence Modelling and Experiments*, Vol. 4, Elsevier, New York, May 1999, pp. 3–18.
[15] Kim, J., and Sung, H. J., "Wall Pressure Fluctuations and Flow-Induced Noise in a Turbulent Boundary Layer over a Bump," *Journal of Fluid Mechanics*, Vol. 558, 2006, pp. 79–102. doi:10.1017/S002211200600989X
[16] Webster, D. R., DeGraaff, D. B., and Eaton, J. K., "Turbulence Characteristics of a Boundary Layer over a Two-Dimensional Bump," *Journal of Fluid Mechanics*, Vol. 320, No. 1, 1996, pp. 53–69. doi:10.1017/S0022112096007458
[17] Hu, Z. W., Morfey, C. L., and Sandham, N. D., "Aeroacoustics of Wall-Bounded Turbulent Flows," AIAA Paper 2001-2172, May 2001.
[18] Mendonça, F., Allen, R., de Charentenay, J., and Lewis, M., "Towards Understanding LES and DES for Industrial Aeroacoustic Predictions," *International Workshop on LES for Acoustics*, DLR, Germany Aerospace Center, Göttingen, Germany, Oct. 2002, pp. 1–8.
[19] Ciardi, M., and Dawes, N., "Development of a Large Eddy and Detached Eddy Simulation Capability for Broadband Noise Prediction on Unstructured Meshes," AIAA Paper 2003-3734, June 2003.
[20] Lee, Y. T., Blake, W. K., and Farabee, T. M., "Prediction of Wall Pressure Spectrum using a RANS Calculation," AIAA Paper 2005-802, Jan. 2005.
[21] Camussi, R., Guj, G., and Ragni, A., "Wall Pressure Fluctuations Induced by Turbulent Boundary Layers over Surfaces of Discontinuities," *Journal of Sound and Vibration*, Vol. 294, Nos. 1–2, 2006, pp. 177–204. doi:10.1016/j.jsv.2005.11.007
[22] Efimtsov, B. M., Kozlov, N. M., Kravchenko, S. V., and Andersson, A. O., "Wall Pressure-Fluctuation Spectra at Small Forward-Facing Steps," AIAA Paper 1999-1964, May 1999.
[23] Efimtsov, B. M., Kozlov, N. M., Kravchenko, S. V., and Andersson, A. O., "Wall Pressure-Fluctuation Spectra at Small Backward-Facing Steps," AIAA Paper 2000-2053, June 2000.
[24] Efimtsov, B. M., Golubev, A. Y., Rizzi, S. A., Andersson, A. O., Rackl, R. G., and Andrianov, E. V., "Influence of Small Steps on Wall Pressure Fluctuation Spectra Measured on TU-144LL Flying Laboratory," AIAA Paper 2002-2605, June 2002.
[25] Strang, W. Z., Tomaro, R. F., and Grismer, M. J., "The Defining Methods of Cobalt60: a Parallel, Implicit, Unstructured Euler/Navier—Stokes Flow Solver," AIAA Paper 99-0786, Jan. 1999.
[26] Forsythe, J. R., Strang, W., and Hoffmann, K. A., "Validation of Several Reynolds-Averaged Turbulence Models in a 3D Unstructured Grid Code," AIAA Paper 2000-2552, June 2000.
[27] Tomaro, R. F., Strang, W. Z., and Sankar, L. N., "An Implicit Algorithm for Solving Time Dependent Flows on Unstructured Grids," AIAA Paper 97-0333, Jan. 1997.
[28] Cobalt, Software Package, Ver. 3.0, Cobalt Solutions, LLC, Springfield, OH, 2003.
[29] Polsky, S. A., and Bruner, C. W. S., "Time-Accurate Computational Simulations of an LHA Ship Airwake," AIAA Paper 2000-4126, Aug. 2000.
[30] Spalart, P. R., Jou, W.-H., Strelets, M., and Allmaras, S. R., "Comments on the Feasibility of LES for Wings, and on a Hybrid RANS/LES Approach," *Advances in DNS/LES, 1st AFOSR International Conference on DNS/LES*, Greyden, Columbus, OH, 1997, pp. 137–148.
[31] Travin, A., Shur, M., Strelets, M., and Spalart, P., "Detached-Eddy Simulations Past a Circular Cylinder," *Flow, Turbulence and Combustion*, Vol. 63, No. 1, 2000, pp. 293–313. doi:10.1023/A:1009901401183
[32] Driver, D. M., and Seegmiller, H. L., "Features of a Reattaching Turbulent Shear Layer in Divergent Channel Flow," *AIAA Journal*, Vol. 23, No. 2, 1985, pp. 163–171. doi:10.2514/3.8890
[33] Driver, D. M., Seegmiller, H. L., and Marvin, J. G., "Time-Dependent Behavior of a Reattaching Shear Layer," *AIAA Journal*, Vol. 25, No. 7, 1987, pp. 914–919. doi:10.2514/3.9722
[34] Magagnato, F., Pritz, B., and Gabi, M., "Comparison of DES and LES on the Transitional Flow of Turbine Blades," *Second Symposium on Hybrid RANS-LES Methods*, 2007, Springer, New York, pp. 212–221.